Received: 15 September 2023 | Revised: 1 November 2023 | Accepted: 4 November 2023

DOI: 10.1002/bit.28601

ARTICLE

BIOTECHNOLOGY AND BIOENGINEERING WILEY

Pushing the boundaries of phosphorylase cascade reaction for cellobiose production II: Model-based multiobjective optimization

Alexander Sigg[1] | Mario Klimacek[1] | Bernd Nidetzky[1,2]

[1]Institute of Biotechnology and Biochemical Engineering, Graz University of Technology, NAWI Graz, Graz, Austria

[2]Austrian Centre of Industrial Biotechnology (acib), Graz, Austria

Correspondence
Bernd Nidetzky, Institute of Biotechnology and Biochemical Engineering, Graz University of Technology, NAWI Graz, Petersgasse 12, A-8010 Graz, Austria.
Email: bernd.nidetzky@tugraz.at

Funding information
European Union's Horizon 2020, Grant/Award Number: 761030

Abstract

The inherent complexity of coupled biocatalytic reactions presents a major challenge for process development with one-pot multienzyme cascade transformations. Kinetic models are powerful engineering tools to guide the optimization of cascade reactions towards a performance suitable for scale up to an actual production. Here, we report kinetic model-based window of operation analysis for cellobiose production (≥100 g/L) from sucrose and glucose by indirect transglycosylation via glucose 1-phosphate as intermediate. The two-step cascade transformation is catalyzed by sucrose and cellobiose phosphorylase in the presence of substoichiometric amounts of phosphate (≤27 mol% of substrate). Kinetic modeling was instrumental to uncover the hidden effect of bulk microviscosity due to high sugar concentrations on decreasing the rate of cellobiose phosphorylase specifically. The mechanistic-empirical hybrid model thus developed gives a comprehensive description of the cascade reaction at industrially relevant substrate conditions. Model simulations serve to unravel opposed relationships between efficient utilization of the enzymes and maximized concentration (or yield) of the product within a given process time, in dependence of the initial concentrations of substrate and phosphate used. Optimum balance of these competing key metrics of process performance is suggested from the model-calculated window of operation and is verified experimentally. The evidence shown highlights the important use of kinetic modeling for the characterization and optimization of cascade reactions in ways that appear to be inaccessible to purely data-driven approaches.

KEYWORDS
cascade bio-catalysis, cellobiose, disaccharide phosphorylases, hybrid-kinetic modeling, multiobjective optimization, process intensification, window of operation analysis

Abbreviations: Cb, cellobiose; CbP, cellobiose phosphorylase; Fru, D-fructose; G1P, α-D-glucose 1-phosphate; Glc, D-glucose; Pi, phosphate; ScP, sucrose phosphorylase; Suc, sucrose.

1 | INTRODUCTION

Cascade transformations by coupled disaccharide phosphorylases (Figure 1) have promising uses in the production of carbohydrate-based ingredients (e.g., di- and oligosaccharides, glycosides; Kadokawa, 2016; Luley-Goedl & Nidetzky, 2010; Pergolizzi et al., 2017). The enzymes are, in general, highly active and robust catalysts. The products of their reactions often achieve significant valorization of expedient bulk sugar substrates (Kitaoka, 2015; Nishimoto, 2020; Ubiparip et al., 2021). Cellobiose has attracted considerable interest for use as additive in different food and feed applications (Brucher & Häßler, 2019; Kitaoka et al., 1992; Schwaiger et al., 2020; Suzuki et al., 2009; Wang et al., 2022). Its bottom-up synthesis from sucrose and glucose involves a one-pot cascade reaction of sucrose phosphorylase (ScP) and cellobiose phosphorylase (CbP), as shown in Figure 1. An industrial process for cellobiose production by coupled ScP and CbP has been implemented at SAVANNA Ingredients (Germany) and is currently developed to full manufacturing scale (Brucher & Häßler, 2019). Process intensification thus becomes an essential task during the scale up to ensure cost effectiveness of the commercial production.

The cellobiose process exemplifies characteristically the fundamental challenges that arise during the optimization of multienzyme cascade transformations (Kara & Rudroff, 2021; Siedentop et al., 2021; Teshima et al., 2023; You & Percival Zhang, 2017). Basic requirements of reaction efficiency, such as product concentration, product yield (*Y*), space-time yield (STY) and productivity of enzyme catalysts must be met for industrial suitability of the biocatalytic process (Domínguez de María, 2021; Lange, 2021; Sheldon & Woodley, 2018; Siedentop & Rosenthal, 2022; Woodley, 2022). Optimization of reaction variables (e.g., concentrations, concentration ratios, time) is rendered difficult technically because each parameter of efficiency of the overall transformation is composite of the interconnected outputs of the individual reactions telescoped in one pot (Kara & Rudroff, 2021; Siedentop et al., 2021). Optimization is even more complicated as it usually involves significant trade-offs between multiple competing objectives (Dvorak et al., 2014; Johannsen et al., 2021; Paschalidis et al., 2022), such as maximum product yield and minimum enzyme usage, for example. Lastly, there can be substantial variation in the expectation of optimization capability, depending on the progress of process development and scale up (Teshima et al., 2023; Wang et al., 2020). While chemical intuition provides useful guidance in each step, comprehensive optimization requires rigorous methodologies based on systematic workflows and robust strategies (Abt et al., 2018; Duong-Trung et al., 2023; Helleckes et al., 2023; Kuschmierz et al., 2022; Pandi et al., 2022; Petroll et al., 2019; Siedentop et al., 2021). Here, we demonstrate the proficiency of an unbiased (nonalgorithmic) approach that applies flexible window of operation analysis (Woodley, 2022) constructed on the results of a mechanistic model-based assessment of the full parameter space of the phosphorylase cascade reaction for cellobiose production.

There has lately been considerable interest across the (bio) chemical sciences in the application of algorithm-based methodologies for the optimization of multistep reactions for synthetic transformations (Taylor, Felton, et al., 2023; Taylor, Pomberger, et al., 2023; Zhou et al., 2017). Powered by machine learning, the process was shown to be automatable in variable degree so as to

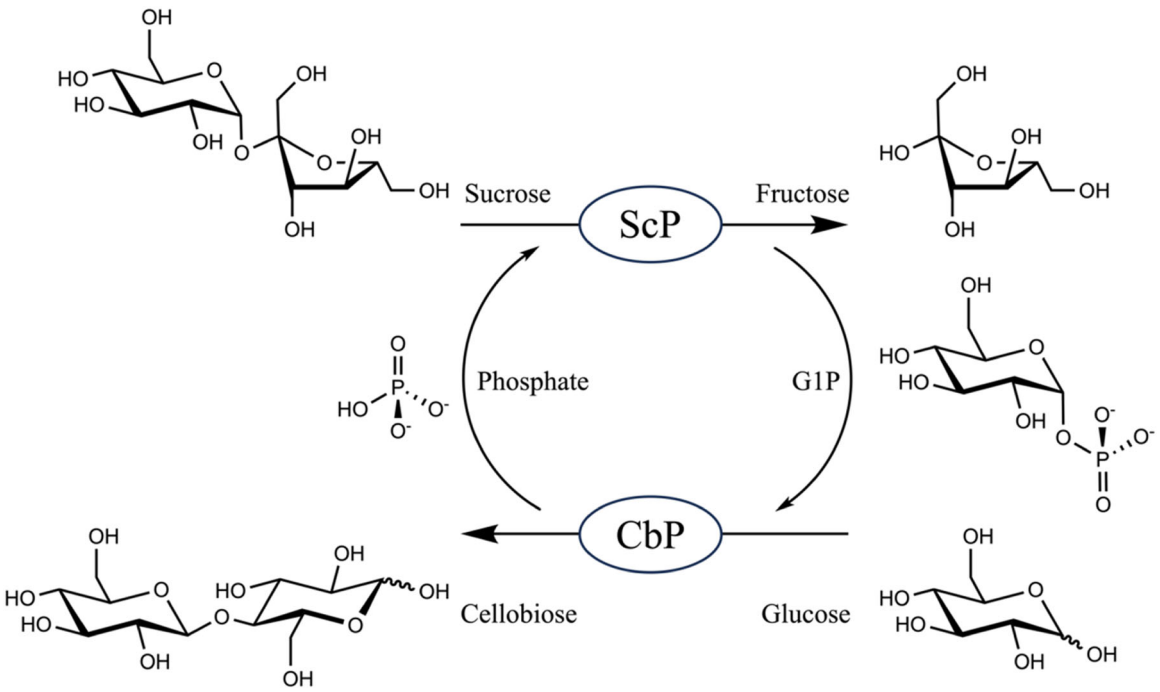

FIGURE 1 Reaction scheme for cellobiose synthesis. CbP, cellobiose phosphorylase; ScP, sucrose phosphorylase.

enable even self-optimization (Clayton et al., 2020; Duong-Trung et al., 2023; Fitzpatrick et al., 2016; Taylor, Pomberger, et al., 2023). It is widely appreciated that an approach based on experienced human intuition, typically involving iterative variation of a single factor at a time, is generally rather inefficient for reaction optimization. A more robust approach uses design of experiments which can be performed in a purely data-driven fashion based on statistical models or under support from kinetic models of the synthetic reactions (Siedentop et al., 2021; Taylor, Pomberger, et al., 2023). Mechanism-based kinetic models achieve the most comprehensive and in-depth description of the reactions analyzed (Almquist et al., 2014; Gernaey et al., 2010; Harris et al., 2022; Sigg et al., 2021, 2023). These models are powerful engineering tools of optimization in their own right. They enable computer simulation to explore the relevant reaction parameter space in a comprehensive manner and in ways that are unbiased by the search for predefined optimum operational points (Lagerman et al., 2022; Lencastre Fernandes et al., 2013). Multi-objective optimization often requires prioritization of single objectives based on prior judgment of the relative importance of a particular trade-off between certain competing objectives (Paschalidis et al., 2022; Rosa et al., 2022; Siedentop et al., 2023). Alternatively, the full set of trade-offs can be considered in a so-called Pareto optimization which identifies a set of best compromises. The Pareto front is thus defined as a set of points in which improvement in one objective results in the deterioration of another. However, even in Pareto optimization it becomes necessary to preselect constraints on objectives based on a priori judgments. These judgments may not always be objective and clear and additionally, they can result in important parts of the parameter space to remain unexplored (Taylor, Pomberger, et al., 2023).

Here, we show an unconstrained approach of kinetic modeling for the optimization of the coupled phosphorylase reaction for cellobiose synthesis. Optimization is here understood as the flexible identification of a suitable window of operation to fulfill different processing objectives. Kinetic simulation combined with experimental validation was furthermore instrumental to uncover a crucial, but hidden mechanistic detail of the cascade reaction: the rate of CbP is decreased by the effect of bulk microviscosity due to high sugar concentrations. The viscosity effect becomes a dominant factor of overall reaction efficiency at the substrate conditions of the industrial process. Based on modeling work by Sigg et al. (2023) in the accompanying paper, a new hybrid (mechanistic-empirical) model was developed here to obtain comprehensive description of the output of the cascade reaction under all conditions used. Based on window of operation analysis enabled by simulations with this new model, different scenarios are identified for optimum production and are verified experimentally. The evidence here shown emphasizes the important use of kinetic modeling for the characterization and optimization of cascade reactions in ways that appear to be inaccessible to mainly data-driven approaches.

2 | MATERIALS AND METHODS

2.1 | Experimental procedures

Unless mentioned otherwise, experiments were performed using materials and procedures exactly as described in the accompanying paper (Sigg et al., 2023). α,α-Trehalose was from Carl Roth.

2.2 | Kinetic modeling

The kinetic model M4 of Sigg et al. (2023) was used as point of departure. For further expansion of model M4, the King–Altmann method was used to derive rate equations of the kinetic mechanism considered. Grouping of microscopic rate constants into kinetic parameters was done according to literature (Segel, 1993). Model fitting was done with COPASI 4.34 (Build 251) as described in Sigg et al. (2023) and applying the specific constraints detailed under Results and Discussion. Parameter sensitivity and goodness of fit R^2 were used to assess model quality and accuracy. Window of operation analysis was performed based on simulations of reaction time courses created with the parameter scan tool embedded in COPASI. Numerical reaction variables (enzyme and substrate concentrations) were varied systematically for simulation and relevant parameters of reaction efficiency were calculated from the resulting time courses described later. Results were visualized graphically and selected conditions of optimum performance of the reaction were verified experimentally in conversion experiments.

3 | RESULTS AND DISCUSSION

3.1 | A hidden factor of cascade reaction efficiency

Kinetic model M4 developed in Sigg et al. (2023) was used for reaction optimization. The objectives were set as follows: product concentration ≥ 500 mM; product yield ≥ 0.9; and reaction time ≤ 48 h. The minimum total amount of volumetric activity, or protein, of both enzymes (ScP + CbP; U/mL or mg/mL) necessary to meet the objectives was identified through window of operation analysis (Supporting Information: Figure S1). To release Cb in the concentration targeted, a minimum activity of 10 U/mL was required (Supporting Information: Figure S1A). The CbP/ScP activity ratio consistent with the processing objectives varied in the range 3:2–4:1 (Supporting Information: Figure S1B). In the enzyme preparations used, the specific activity of ScP (47 U/mg) exceeded that of CbP by 4.3-fold. The total amount of protein used in the reaction was therefore minimal (~1.2 mg/mL) when the CbP activity (8.0 U/mL) surpassed the ScP activity (2.0 U/mL) by approximately fourfold. The requirement for excess CbP activity can be understood from the strong substrate inhibition of the enzyme by glucose, as implemented in model M4 (Sigg et al., 2023). Conditions marked in Supporting Information: Figure S1 (panel C: 650 mM Suc and Glc; panel D:

TABLE 1 Reaction conditions of conversion experiments.

		Fitting					
		A	B	C	D	E	F
ScP	[U·ml^{-1}]	1.50	7.77	11.6	11.6	25.2	2.00
CbP	[U·ml^{-1}]	0.75	0.75	1.52	1.52	8.93	8.00
$[Suc]_0$	[mM]	100	300	300	500	600	650
$[Glc]_0$	[mM]	100	300	300	200	600	650
$[Pi]_0$	[mM]	9.13	39.0	80.0	39.0	10.0	80.0
		Validation					
		A	B	C	D		
ScP	[U·ml^{-1}]	1.18	9.72	11.6	11.6		
CbP	[U·ml^{-1}]	0.76	1.52	1.52	1.52		
$[Suc]_0$	[mM]	100	300	300	200		
$[Glc]_0$	[mM]	100	300	300	500		
$[Pi]_0$	[mM]	9.13	39.0	71.0	39.0		
		Multiobjective analysis					
		MA 1	MA 2	MA 3			
ScP	[U·ml^{-1}]	8.30	10.0	38.0			
CbP	[U·ml^{-1}]	2.40	2.80	4.80			
$[Suc]_0$	[mM]	360	340	340			
$[Glc]_0$	[mM]	360	340	340			
$[Pi]_0$	[mM]	35.0	27.5	12.5			
Y_{Cb}	[–]	0.80	0.85	0.90			
Cb/CbP	[µmol/U]	122	107	64			

Abbreviations: CbP, cellobiose phosphorylase; ScP, sucrose phosphorylase.

80 mM Pi) and shown in Table 1 (entry F) were selected for experimental verification and results are shown in Figure 2a.

Predictions of model M4 differed widely from the experiment, especially in the early phase of the reaction (≤3 h) where the actual conversion rate was 3.5-fold lower than expected from the simulation. Considering possible factors of rate retardation not captured by model M4, we excluded inhibition by Glc as it is already incorporated in the mechanistic description. We also excluded product inhibition for the reasons that the model deviates from experiment under conditions when the product release is still low (Figure 2a) and earlier validations of model M4 have been done in experiments involving similar amounts of Cb and Fru formed. We therefore concluded that model deviation must arise from inhibitory effect introduced by substrate (Suc, Pi) other than Glc or by the intermediary G1P. To achieve clarification, we performed initial-rate kinetic studies in which the substrate conditions were varied systematically and the individual enzymatic rates were measured. As shown in Figure 2, predictions of model M4 were in excellent agreement with the experimental rates of ScP whereas they failed in large extents to reproduce the rates of CbP. Significantly, a doubling of [Suc] from 300 to 600 mM resulted in a CbP rate reduction by 40%–65%, independent of the [G1P] present in the reaction (Figure 2c). Relationship between [Suc] and degree of apparent inhibition of CbP was thus suggested.

In search of reasons for a major effect of [Suc] on the CbP rate missed in the earlier study of Sigg et al. (2023), we analyzed from time course simulations how the individual enzymatic rates, and the degree of utilization of the maximum activity of CbP and ScP, changed in dependence of the substrate conversion. Reaction conditions A–F in Table 1 were simulated and plots of volumetric CbP/ScP rate ratio are shown in Figure 3a. The general trend is that the cascade reactions start from a CbP/ScP rate ratio substantially smaller than unity, implying limitation of the overall transformation rate by the CbP rate initially. The ratio quickly increases to a value of approximately 1 that remains constant during the further conversion. The exception of reaction E is explained by high enzyme concentrations used in combination with low [Pi], so that balancing of the CbP and ScP rates happened within the time interval used for calculation of the rate ratio. We also determined the specific enzymatic rates at each point of the reaction and related them to the maximum rate of the individual enzyme. The resulting ratio expresses the degree in which the respective enzyme is utilized in the reaction. Results in Figure 3b show that the optimized reaction F differs from all other reactions (A–E) in that the CbP activity was less completely utilized than the ScP activity. The situation is reversed (i.e., ScP activity less completely utilized) in the other reactions. The optimized reaction thus involves unmasking of CbP inhibition in a degree considerably larger than in reactions used to establish model M4.

3.2 | Inhibition by specific binding of sucrose excluded

Supporting Information: Figure S2 shows a kinetic mechanism of CbP in which all conceivable binding modes of Suc to the enzyme were considered. Given the fact that the CbP binding pocket contains two subsites for sugar binding (Kitaoka et al., 1992; Nidetzky et al., 2000; Van Hoorebeke et al., 2010), Suc binding was likely to occur to the free enzyme, but alternative binding modes could not be excluded at this stage. A full steady-state kinetic model of the Suc-inhibited CbP is presented in Supporting Information: Table S1. The complete model of the cascade reaction which includes the kinetic description of the ScP reaction (Supporting Information: Table S2, identic with M4 from Sigg et al., 2023) is referred to as M5 to follow the kinetic model numbering of Sigg et al. (2023). Model M5 was fitted to time courses A–E of Table 1 using the results of initial rate studies in Figure 2 as additional constraints. Supporting Information: Table S3 shows the parameter estimates along with the complete set of boundaries and constraints used for fitting. Supporting Information: Table S4 shows the reaction variables as optimized by fitting. Model M5 gave an excellent representation of the experimental time courses, as shown in Supporting Information: Figure S3. The initial rate data could also be described well (Supporting Information: Figure S4). However, the time course F used for validation could not be reproduced in suitable quality (Supporting Information: Figure S3F). Of the different binding modes of Suc

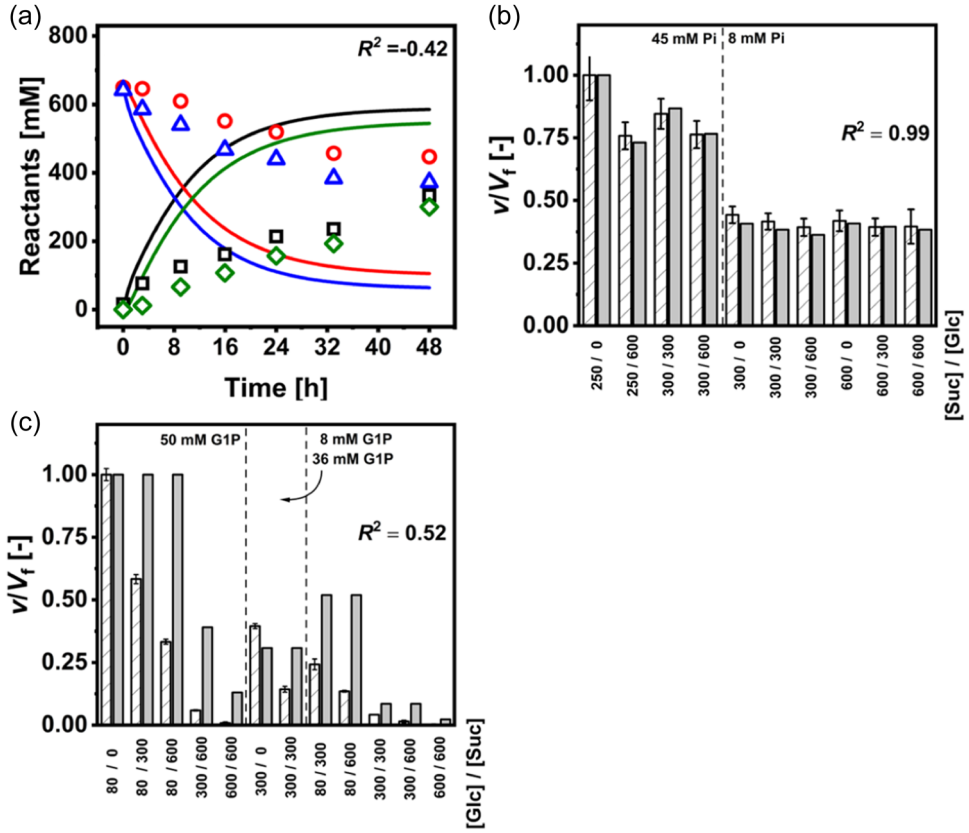

FIGURE 2 Assessment of model M4 in time-course and initial-rate studies. (a) Experimental verification of the operational optimum predicted by the model (see Table 1, entry F; Figure S1 (Supporting Information), panels c and d). Symbols show the experimental data (Suc, triangles; Glc circles; Fru, squares; Cb, diamonds), lines show the simulation. (b) and (c) Initial rates relative to V_f of ScP (b) and CbP (c) at different compositions of the reaction mixture. Data are from two independent experiments, shown as shaded bars with error bars indicating the standard deviation. The corresponding model simulations are shown as grey bars with goodness of fit (R^2) indicated. CbP, cellobiose phosphorylase; ScP, sucrose phosphorylase.

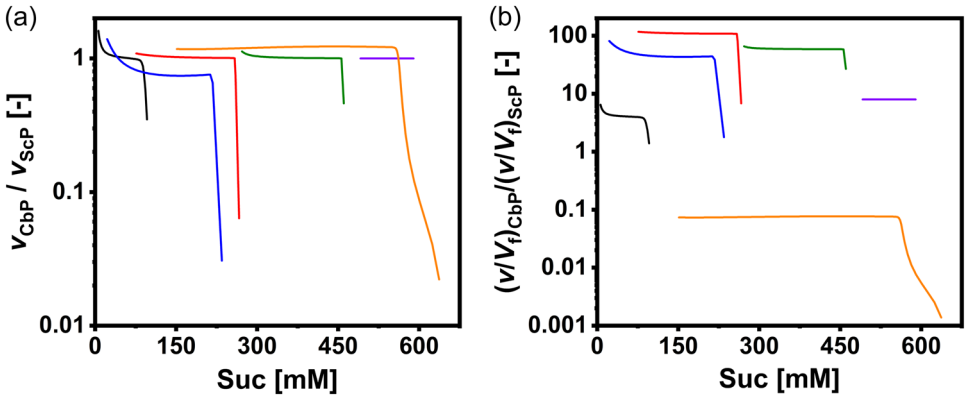

FIGURE 3 Simulations of model M6 to identify rate limitation and efficiency of enzyme utilization in different conditions of the cascade reaction. (a) The ratio of volumetric rates (v) of CbP and ScP are shown in dependence of [Suc] present in the reaction. (b) The relative efficiency of enzyme utilization is the ratio of the volumetric rates of CbP and ScP, each normalized on the maximum rate (V_f) of the respective enzyme. Lines show simulation data of model M6 with reaction conditions according to Table 1 (black, A; red, B; blue, C; green, D; purple, E; orange, F). CbP, cellobiose phosphorylase; ScP, sucrose phosphorylase.

considered in Supporting Information: Figure S2, only the binding to free enzyme (K_{iSuc1}) was potentially significant in terms of binding strength (Supporting Information: Table S3). However, parameter estimate for K_{iSuc1} was linearly correlated with estimates for inhibition constants of glucose, in particular that of K_{iGlc3}. It was not possible, therefore, to distinguish between inhibition of CbP due to binding of Glc or Suc, solely based on model M5 fits to the time course data. However, evidence from initial rate studies (Supporting Information: Figure 2c), that CbP inhibition by Suc was similar irrespective of the degree of enzyme saturation with G1P (8.0 mM, 2.6 K_{G1P}; 50 mM, 16 K_{G1P}), cast doubt on the idea of Suc binding to the free CbP and suggested that alternative (bulk) effects of high [Suc] on the enzyme activity be considered.

3.3 | Bulk microviscosity uncovered as a critical factor of enzymatic rate limitation

A prominent way for high sugar concentrations to influence enzyme activity is through their effect on bulk microviscosity. Physical steps of enzyme catalysis, in particular those involving dynamical rearrangements of the protein structure, can be sensitive to changes in the microviscosity (Sampedro et al., 2020). We here performed initial rate experiments using α,α-trehalose as a small-molecule microviscogen that is unreactive with both CbP and ScP. Of note, dependence of fluid microviscosity on the mass-based concentration is identical for α,α-trehalose and the sugar compounds of the cascade reaction (Glc, Suc, Fru, Cb; Galmarini et al., 2011; Telis et al., 2007). Viscosity of G1P was assumed to be similar to the one of Glc. Results in Figure 4a reveal CbP activity lowered in a roughly linear fashion dependent on the total reactant concentration in the mixture. Measurements performed at saturating (50 mM) and nonsaturating concentrations (8.0 mM) of G1P in the presence of 80 mM Glc do not give the same slope, as expected because the distribution of enzyme forms at steady state is not identical for the two conditions, but the linear dependence of decline in rate on reactant concentration remains. Effect of the reactant concentration (Figure 4a) can also be expressed in terms of change of microviscosity caused, as shown in Supporting Information: Figure S5. Plausible interpretation of the viscosity effect is according to Kramer's theory: the transmission coefficient for virtual barrier crossing in the rate-limiting step of the overall CbP catalysis (k_{cat}) depends inversely on the solvent friction (Sampedro et al., 2020). On this interpretation, an empirical extension of model

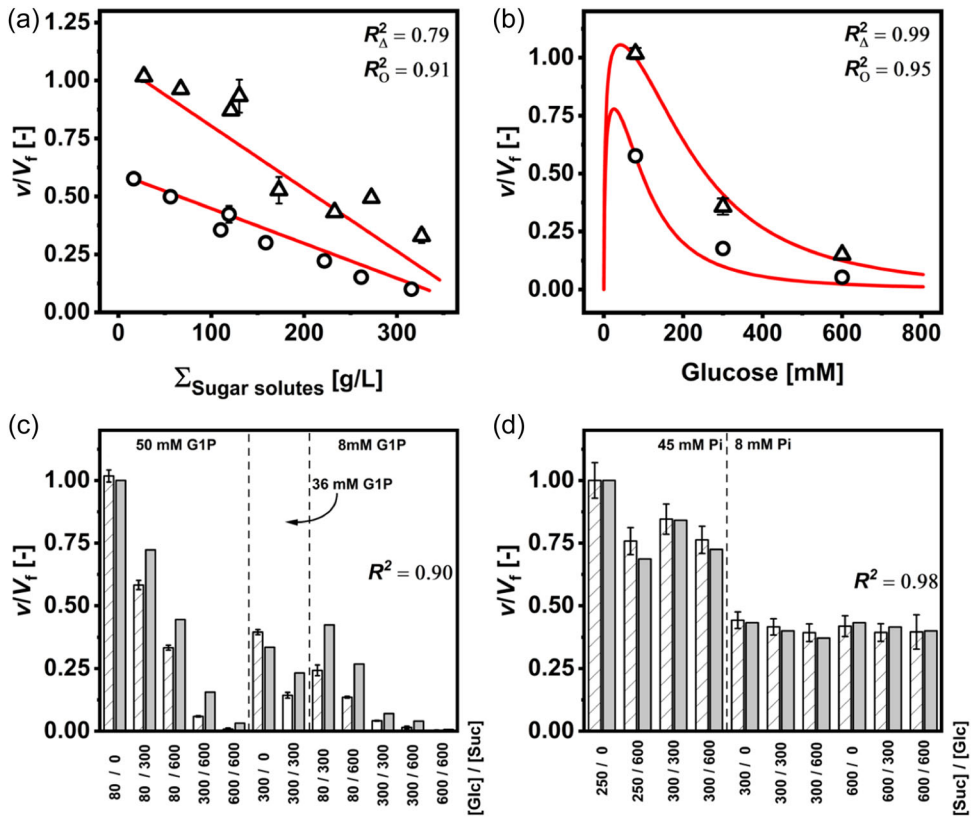

FIGURE 4 Results of initial rate analysis for CbP (a–c) and ScP (d) using model M6. (a) Effect of the total concentration of sugar solutes on the enzymatic rate. Symbols show the data (Glc/G1P: 80 mM/50 mM, triangles; 80 mM/8 mM, circles; each with and without varied concentrations of α,α-trehalose added) and solid lines show the simulation results (averages of 10 fits). (b) Simulation of the Glc inhibition on CbP. Symbols show the data (G1P: 50 mM, triangles; 8.0 mM, circles) and lines show the fit. Data are from Sigg et al. (2023). (c) and (d) Effect of Glc and Suc on initial rate of CbP (c) and ScP (d) reaction. Shaded bars show the data and grey bars show the simulation. Error bars are standard deviations of duplicate experiments. CbP, cellobiose phosphorylase; ScP, sucrose phosphorylase.

TABLE 2 Summary of the developed kinetic model M6 for ScP and CbP.

ScP

$$v = \frac{V_f[Suc][Pi]}{K_{Suc}[Pi]\left(1+\frac{[Glc]}{K_{iGlc}}\right)+K_{Pi}[Suc]+[Suc][Pi]}\left(1-\frac{\frac{[G1P][Fru]}{[Suc][Pi]}}{K_{eq}}\right)$$

CbP

$$v_{CuCbP} = v_{mechanistic}\cdot BE = \frac{V_f\cdot BE\cdot[G1P][Glc]}{D}\left(1-\frac{\frac{[Pi][Cb]}{[G1P][Glc]}}{K_{eq}}\right)$$

$$BE\begin{cases}\sum(M_{W,i}\cdot c_i) < 27.4\frac{g}{L};\ BE = 1\\ \sum(M_{W,i}\cdot c_i) \geq 27.4\frac{g}{L};\ BE = 1+m\cdot\left(\sum(M_{W,i}\cdot c_i)-x\right)\end{cases}$$

$$\begin{aligned}D = {} & K_{iG1P}K_{Glc}\left(1+\frac{[Glc][Pi][Cb]}{K_{iCb}K_{Pi}K_{iGlc1}}+\frac{K_{Cb}[Glc]^2[Pi]}{K_{iCb}K_{Pi}K_{iGlc2}K_{iiGlc3}}+\frac{[Pi][Cb]}{K_{iCb}K_{Pi}}\right.\\ & \left.+\frac{K_{Cb}[Glc][Pi]}{K_{iCb}K_{Pi}K_{iGlc2}}+\frac{[Glc]^2}{K_{iGlc2}K_{iGlc3}}+\frac{K_{Cb}[Pi]}{K_{iCb}K_{Pi}}+\frac{[Cb]}{K_{iCb}}+\frac{[Glc]}{K_{iGlc2}}\right)\\ & +K_{G1P}[Glc]\left(1+\frac{[Glc]^2}{K_{iGlc2}K_{iGlc3}}+\frac{[Cb]}{K_{iCb}}+\frac{[Glc]}{K_{iGlc2}}\right)+\frac{[G1P][Glc][Pi]}{K_{iPi}}\\ & +K_{Glc}[G1P]\left(1+\frac{K_{Cb}[Pi]}{K_{iCb}K_{Pi}}\right)+[G1P][Glc]\end{aligned}$$

Note: Definitions of kinetic parameters are summarized in Supporting Information: Tables S2 and S5 for ScP and CbP, respectively.

Abbreviations: *BE*, nonspecific bulk effects; *c*, concentrations; Cb, cellobiose; CbP, cellobiose phosphorylase; Fru, fructose; G1P, α-d-glucose 1-phosphate; Glc, glucose; V_f K_{eq}, equilibrium constant; *K*, Michaelis constant; K_i, dissociation constant; *m*, linear dependency of *BE* on dissolved reaction components; M_W, molecular weight; Pi, phosphate; ScP, sucrose phosphorylase; Suc, sucrose; V_f, maximum velocity of the forward direction; *cx*, mass of reaction compounds in the activity assay (50 mM G1P + 80 mM Glc → *x* = 27.4 g/L).

M4 was made to express dependence of the maximum rate of CbP on the total reactant concentration present in the reaction, relative to the reference of the enzyme's maximum rate under standard assay conditions (total reactant concentration: 27.4 g/L).

The resulting model M6 is shown in Table 2 with kinetic parameters being summarized in Supporting Information: Table S2 (ScP reaction) and Supporting Information: Table S5 (CbP reaction). The model was fitted to time course data (Table 1, conditions A–F) using the results of initial-rate measurements as constraints. The parameter estimates are summarized along with the relevant boundaries and constraints used in Supporting Information: Table S6. Supporting Information: Table S4 shows the reaction variables adjusted by fitting. The fitting results are displayed in Figures 4 and 5. Model M6 gave an excellent description of all of the experimental data, well visible in the figures and also indicated by goodness of fit $R^2 \geq 0.90$. Effect of microviscosity was represented very well, as shown in Figure 4a. Here, capability of model M6 to reproduce the differential sensitivity of the CbP rate to microviscosity change under conditions of saturating and nonsaturating concentrations of G1P is certainly worth to be pointed out.

To validate model M6, we used a separate set of 4 independent time courses (Table 1) and compared simulation results with the experiment. Figure 6 shows excellent agreement of model M6 predictions with actual data and therefore verifies model M6 for the purpose of reaction optimization.

3.4 | Unconstrained simulations support multiobjective optimization

Extensive simulations were performed with model M6 to span a fully representative range of substrate and enzyme concentrations. In view of the industrial applicability of the reaction conditions examined (Brucher & Häßler, 2019), we avoided excess of one substrate over the other and the mole ratio of Suc and Glc was therefore fixed at unity. Pi was variable as indicated. Considering a reasonable upper limit of the total protein loading used for the biotransformation (≤15 mg/mL), the enzyme activities were restricted to 100 U/mL for ScP and CbP. A total of 3.6 million individual time courses was simulated to provide an unconstrained basis for the later selection of optimum. Deepened mechanistic understanding of the cascade reaction, generated through disentanglement of the various interrelated factors of conversion efficiency as discussed below, represents a unique strength of the initially untargeted modeling approach used here. For further analysis, we included reactions reaching product yields (Y_{Cb}) equal to or exceeding the selected target percentage (≥80%–90%; see below) of the thermodynamic maximum yield of Cb (Y_{Cb_eq}) under the conditions used, within 24 h. Note that $Y_{Cb,eq}$ is dependent on the concentration ratio of substrate and Pi and therefore varies in the different reaction conditions. Y_{Cb} was defined according to the relationship $Y_{Cb} = S_{Cb}\cdot X_{Suc}$, where S_{Cb} = [Cb]/([Cb] + [G1P]) is Cb selectivity and X_{Suc} = 1 − ([Suc]/$[Suc]_{t=0}$) is Suc conversion. S_{Cb} accounts for the portion of intermediary G1P not converted into Cb and depends on the initial [Pi] used in the reaction. Simulations fulfilling the Y_{Cb} requirements are displayed in Figure 7 and we use them to identify window of operation for Cb production at 100–200 g/L.

3.4.1 | Reactant concentrations and enzyme loading

Figure 7a illustrates the dependence of Y_{Cb} ($\geq 0.9\ Y_{Cb\_eq}$) on the substrate concentration and does so for different concentrations of Pi. The results reveal the interplay of opposed effects of [Pi] on the Y_{Cb} and on the overall enzymatic activity. Y_{Cb} decreases in general as [Pi] is increased and the effect is strongest at low substrate concentration. For high substrate concentration when [Pi] is low, there are only few reaction conditions, typically involving use of a large amount of enzyme (CbP ≥ 50 U/mL; ScP ≥ 14.4 U/mL), that can satisfy the requirement of $Y_{Cb} \geq 0.9$. To produce Cb at 200 g/L, we took from Figure 7a (Pareto front at $Y_{Cb} = 0.9$) that reaction at 650 mM substrate and 25 mM Pi would be optimal for realization of the set conversion task at a minimized substate and enzyme load.

A common problem for the optimization of enzyme cascade transformations, and catalytic reactions in general, is to prevent that the given processing objective (e.g., space-time yield) is optimized by simply

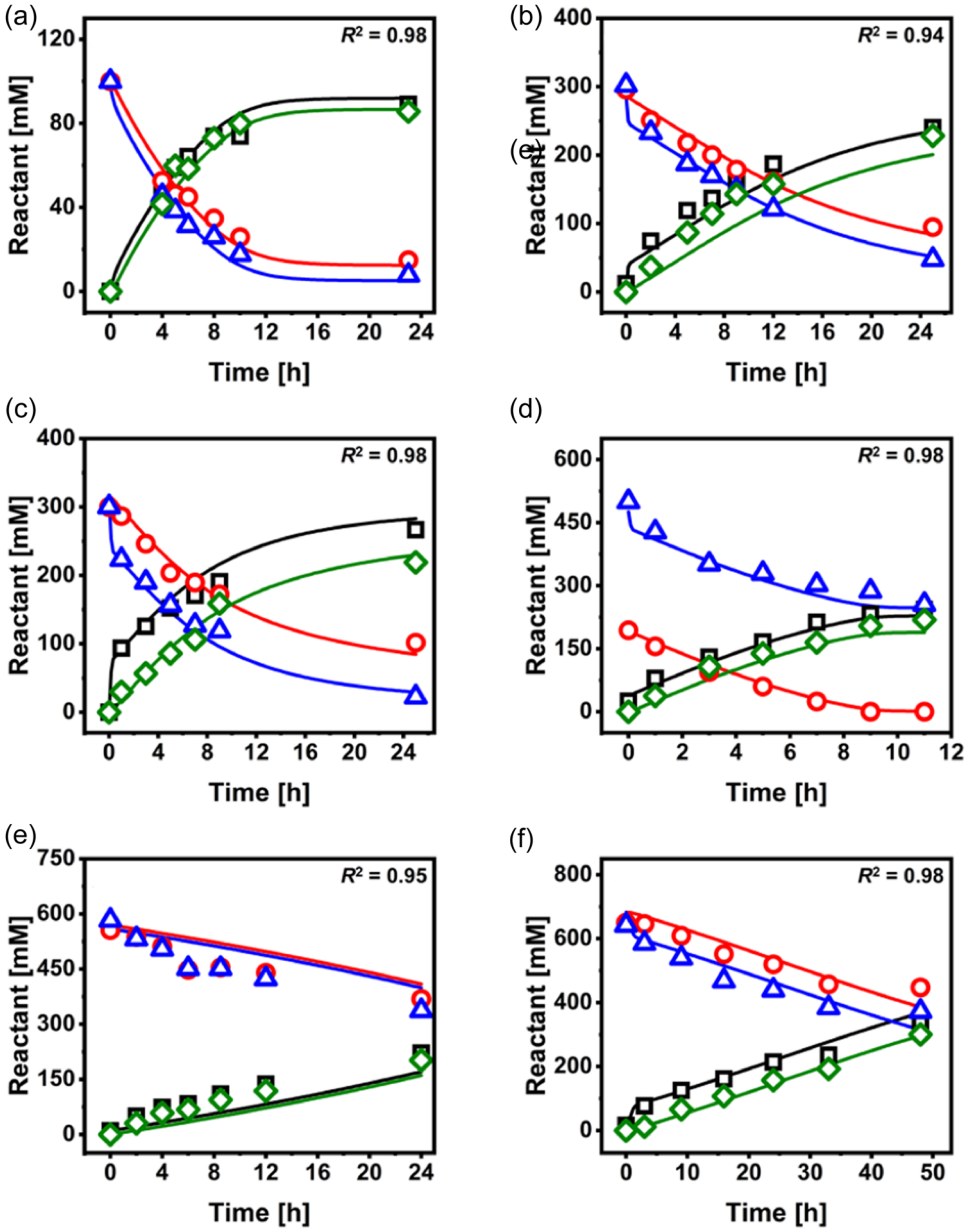

FIGURE 5 Best-fit results of model M6. Panels are labeled according to Table 1 ("Fitting") which identifies the reaction conditions applied. Symbols show the data (Suc, triangles; Glc circles; Fru, squares; Cb, diamonds) and lines show the fit, with goodness of fit (R^2) indicated. Data in panels (a–e) are taken from Sigg et al. (2023).

adding higher amounts of catalyst (Siedentop et al., 2021; Taylor, Pomberger, et al., 2023). We therefore considered here the minimum usage of enzyme consistent with the desired reaction efficiency. Figure 7b shows the [Cb] released in 24 h from reactions giving $Y_{Cb} \geq 0.8\ Y_{Cb_{eq}}$ in dependence of the volumetric activities of CbP and ScP used. The most striking point of Figure 7b is the extremely nonlinear relationship between [Cb] released and CbP activity used. Compared to just 1 U/mL needed to produce 200 mM, a 50-fold larger activity of the CbP is necessary for production of 585 mM (200 g/L). The peculiar behavior of the reaction is explained by substrate and product inhibition in combination with effect of bulk microviscosity on the CbP activity at high substrate concentration. The achievable [Cb] approaches plateau regardless of the amount of enzyme added, indicating important trade-off between production efficiency in terms of the product titer and usage efficiency of the enzyme catalyst. Figure 7b and in detail Supporting Information: Figure S6 reveal furthermore that under a vast majority of the reaction conditions simulated, the ScP activity could be kept at ≤ 10 U/mL to still meet the required conversion task. Only if the production is pushed to the maximum of [Cb] (upper front of the landscape in Figure 7b and back of Supporting Information: Figure S6) does the demand for ScP activity increase to 30 U/mL or higher. ScP is by far less vulnerable to inhibition than CbP. The added requirement for ScP activity is thus explained by the effect of enhanced supply of G1P on the efficiency of the CbP reaction.

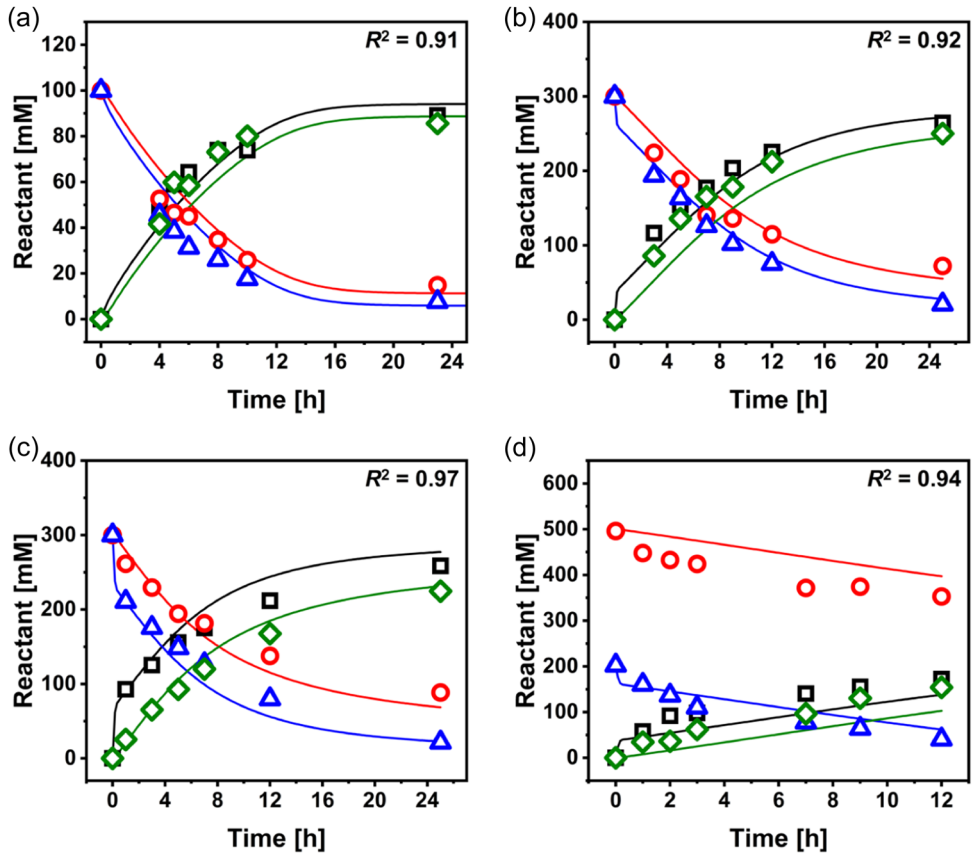

FIGURE 6 Validation of model M6. Panels are labeled according to Table 1 ("Validation") which identifies the reaction conditions used. Lines show the model simulation, symbols show the experimental data (Suc, triangles; Glc circles; Fru, squares; Cb, diamonds) taken from Sigg et al. (2023), with goodness of fit (R^2) indicated.

3.4.2 | Trade-off between Cb release and efficient use of CbP

The ratio of [Cb] released and CbP activity loaded (µmol Cb/U CbP) is used as parameter describing the efficiency of enzyme use in the production. Figure 7c shows this efficiency for simulated reactions with both substrate and Pi concentration varied. Maximum is found at 425 µmol/U achieved at conditions (60 mM substrate,10 mM Pi) that largely exclude effects of inhibition and microviscosity. Reaction identified for Cb production at 200 g/L involves just 3% (= 13 µmol/U) of that efficiency. Contour lines are drawn in Figure 7c at different [Cb] in the range 50–200 g/L and show the associated enzyme efficiencies. Downstream processing of the reaction mixture involves crystallization as the main step of purification and formulation of the Cb (Shimada et al., 2009). The requirement of [Cb] to be at ≥ 500 g/L for crystallization illustrates critical trade-off between the objectives of production at maximum enzyme efficiency and product release optimally aligned to the conditions of downstream processing.

For further analysis, we considered Cb produced at approximately 100 g/L to represent a plausible compromise between the two objectives, involving increase in product concentration compared to the point of maximum enzyme efficiency (~21 g/L) and concentration of the product solution for crystallization by the same five-fold factor. Proceeding along the 100 g/L contour line in Figure 7c, we show that the enzyme efficiency ranges from 29–134 µmol/U. Three operational points equally distributed between Y_{Cb} = 0.8 and 0.9 (Table 1; multiobjective reaction analysis) were selected for experimental assessment. Besides verification of the model predictions, the experiments had the goal of demonstrating the production of Cb at minimum usage of enzyme. Additionally, the relationship between the initial [Pi] and the enzyme demand in the reaction could be analyzed. Note that slight deviation from the 100 g/L contour line in Figure 7c is due to a rounding effect in the simulation. Among the three reaction conditions analyzed, reaction MA 1 was found to be most suitable, as it showed the highest enzyme efficiency of 122 µmol/U (Table 1) under the given boundary conditions.

3.4.3 | Effect of Pi

Selected conditions in Table 1 involve the peculiarity that ScP activity is used in 3.5–7.9-fold excess over CbP activity. Considering the results in Figure 7b and the interpretation thereof, that a relatively low ScP activity of ≤ 10 U/mL and smaller than the corresponding CbP activity was sufficient to meet the processing

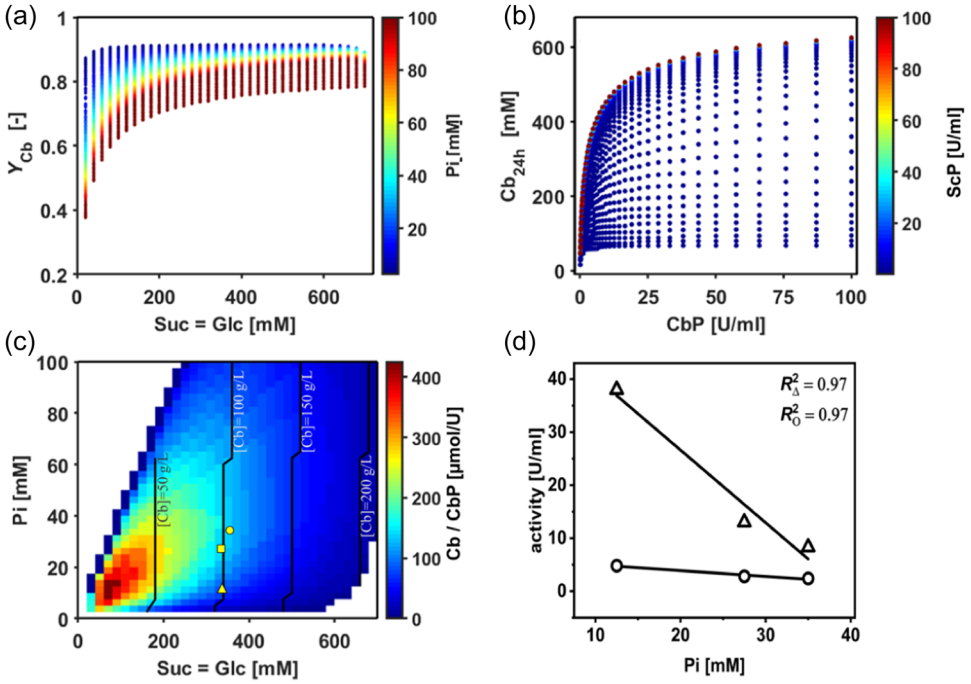

FIGURE 7 Results of window of operation analysis. (a) Influence of initial substrate concentration on Y_{Cb}. (b) Minimum amounts of ScP and CbP needed for Cb production. (c) Influence of initial substrate concentration on catalyst yield (Cb/CbP), with contour lines indicating the achievable Cb concentrations. Symbols show the reaction conditions of multiobjective analysis indicated in Table 1 ("Multiobjective analysis") with triangle showing MA1, square showing MA 2, and circle showing MA 3. (d) Effect of the initial [Pi] on the activity of ScP (triangles) and CbP (circles) required in the optimized reactions MA 1–MA 3 (Table 1). Solid lines show linear regressions with goodness of fits (R^2) indicated. CbP, cellobiose phosphorylase; ScP, sucrose phosphorylase.

objectives, the particular outcome of the optimization warrants discussion. Intuition might suggest that the enzyme more strongly prone to inhibition should be used in excess. Analysis of the simulation data clarifies that the demand for excess ScP arises from effect of the G1P recycling on the overall efficiency of the cascade reaction. The CbP activity benefits from a relatively high steady-state level of the intermediary G1P and the distribution of the initial Pi substrate into G1P and free phosphate depends on the relative rates of the ScP and CbP reactions. Figure 7d shows the requirements for loading of ScP and CbP in the multiobjective analyzed reactions, depending on the concentration of Pi substrate used: the larger the initial [Pi], the lower can be the excess of ScP used. Additionally, the demand of CbP loading decreases 2-fold on increasing the [Pi] from 12 to 35 mM (Figure 7d). Simulations reveal that the steady-state concentration of Pi during the reactions drops to below 1.0 mM which is just about 1/20 the K_{Pi} of ScP. At the optimum operational points of the cascade transformation, therefore, the effect of ScP working at low degree of saturation with Pi is partly compensated by enzyme loading. The results reveal the competing objectives related to the [Pi] used in the reactions: recycling of G1P without limitation is favored at high [Pi], yet this can be achieved only at the expense of Y_{Cb} reduced concomitantly, as discussed above. Kaspar et al. (2020) provide an interesting discussion on the role of [Pi] in transribosylation reactions catalyzed by nucleoside phosphorylase(s).

3.5 | Reaction conditions from multiobjective optimization verified experimentally

Figure 8 shows reaction time courses acquired under the conditions identified in the window of operation analysis based on considerations of multiobjective optimization (Figure 7c and Table 1). The experimental data give excellent agreement with the model predictions. Minor deviation is noted for the concentration of Glc which towards the end of the reaction is higher than predicted. The difference between [Glc] and [Suc] becomes larger than theoretically possible by the mass balance of the coupled enzymatic reactions under the conditions of initial [Pi] used. Note the requirement that $[Glc] - [Suc] \leq [Pi]_0$. The apparent violation of mass balance is explainable by enzymatic hydrolysis of Suc, G1P or both happening in small degree. ScP is known to possess low hydrolase activity towards Suc conditions in which the [Pi] is strongly limiting in the reaction (Klimacek et al., 2020; Sigg et al., 2021). However, as it did not affect the Cb formation, the side reaction leading to excess Glc in the process was not further investigated here.

Table 3 summarizes key performance metrics of the three reactions performed. The Y_{Cb} and [Cb] meet the specific objectives of multiobjective analysis under the respective conditions used. The [Cb] released in reaction MA 1 is below the objective (100 g/L or 292 mM in 24 h), but the immediate measurements of product ([Cb], [Fru]) at the 24 h point appears to be afflicted with error. The overall time course (Figure 8a) is well in agreement with [Cb] formed as

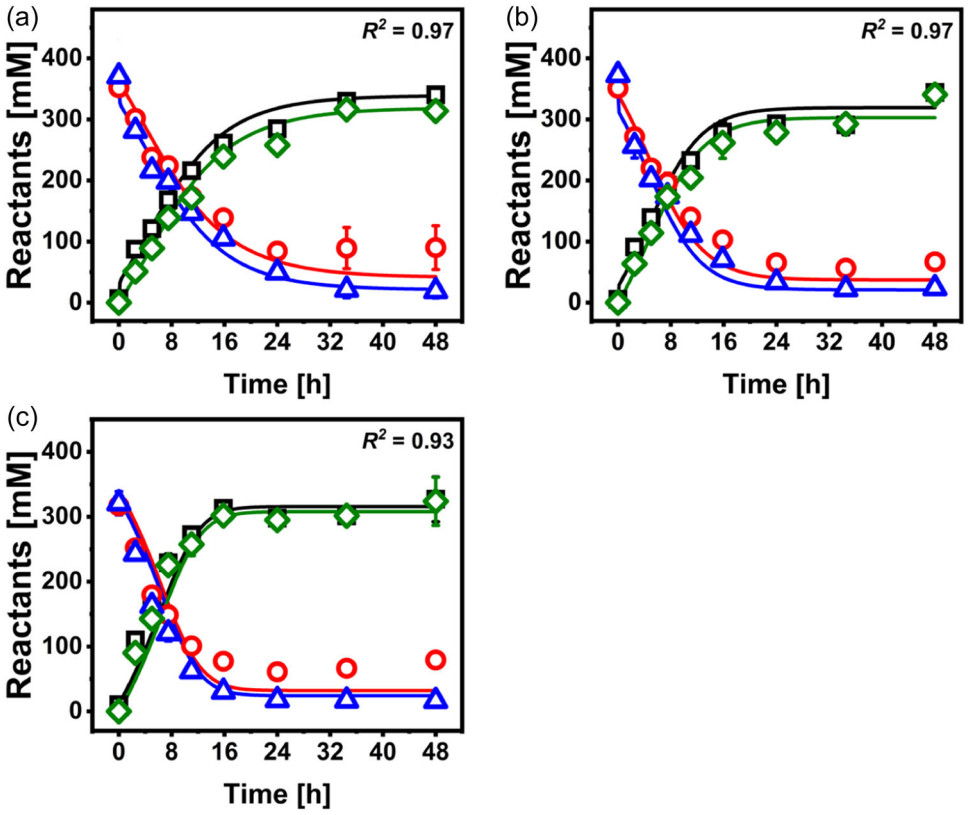

FIGURE 8 Experimental verification of the reaction conditions from multiobjective reaction analysis. Panels are labeled according to Table 1 ("Multiobjective analysis"; a, MA 1; b, MA 2; c, MA3) which identifies the reaction conditions used. Lines show the model simulation, symbols the experimental data (Suc, triangles; Glc circles; Fru, squares; Cb, diamonds) with goodness of fit (R^2) indicated.

TABLE 3 Analysis of the experimental time courses of reactions from multiobjective reaction analysis after 24 h.

Parameter		MA 1	MA 2	MA 3
Y_{Cb}	[-]	0.79 ± 0.07	0.87 ± 0.11	0.93 ± 0.07
Cb	[mM]	257 ± 7	278 ± 13	295 ± 5
Cb/CbP	[µmol/U]	132 ± 14	104 ± 12	62.8 ± 6.4
STY	[mM/h]	10.7 ± 0.3	11.6 ± 0.6	12.3 ± 0.2
$TON_{CbP}\cdot10^5$	[mol/mol]	1.13 ± 0.03	1.04 ± 0.05	0.64 ± 0.01
$TON_{ScP}\cdot10^5$	[mol/mol]	4.69 ± 0.13	4.21 ± 0.20	1.17 ± 0.02

Note: Results represent averages of $N = 2$ experiments with standard deviation indicated. The reaction conditions of MA1–MA3 are from Table 1. The TON values are based on the molar concentrations of Cb product released and enzyme used. The relationship TON = [Cb]/([E]) was used. [E] was calculated from the volumetric enzyme activities, using specific activities (Schwaiger et al., 2022) of 11.4 U/mg and 117 U/mg and molecular masses of 92 kDa (Nidetzky et al., 2004) and 129 kDa (van den Broek et al., 2004) for CbP and ScP, respectively.

predicted by the model. The STY is comparable for all reactions, consistent with the common task of [Cb] release within 24 h. The efficiency of utilization of CbP activity is in accordance with the model predictions and suggests reaction MA 1 (Table 1) to perform most economically among the three reactions used.

The mol-based enzyme turn over numbers (TONs) in the range $0.64–1.13 \times 10^5$ for CbP and $1.17–4.69 \times 10^5$ for ScP are taken to indicate that the enzymatic transformations in batchwise reaction without enzyme recycle proceeded efficiently. In biocatalysis applied to synthesis of simple carbohydrates, enzyme TONs of 10^5 or greater are generally considered to be a requirement for the industrial applicability of the process (Wu et al., 2021). Change of TON (1.7-fold for CbP; 4.0-fold for ScP) in reactions MA 1–3 (Table 1) underlines the important role of [Pi] in determining the reaction performance. Here, the [Pi] does not primarily affect the Y_{Cb} or [Cb] but it changes the minimum enzyme loading (up to four-fold for ScP) necessary to fulfill the objectives of the conversion. The reactions MA 1–3 exemplify trade-off between the objectives of maximized Y_{Cb} and minimized loading of enzymes, both affected by the [Pi] used while achieving the same target value of [Cb].

4 | CONCLUSIONS

Mechanistic-empirical (hybrid) modeling of the ScP-CbP cascade reaction is shown for comprehensive window of operation analysis and multiobjective process optimization of Cb production from Suc and Glc. The modeling approach resulted in the discovery of microviscosity due to high sugar concentration as an important

factor of the bulk solution on the activity of CbP. Modeling was essential to unravel the conflicting relationships between efficient utilization of the enzymes and maximized concentration (or yield) of the product within a given process time and in dependence of the initial concentrations of substrate and phosphate used. Optimum balance of these competing parameters of process performance is revealed by the model-calculated window of operation and is verified in experiments. Our study emphasizes the important use of kinetic modeling for the characterization and optimization of cascade reactions in ways that are likely inaccessible to purely data-driven approaches. We believe that the modeling strategy shown here is broadly applicable to the optimization of enzyme cascade reactions and has relevance in particular when the recycled substrates (here: G1P) must be present in not just catalytic amounts.

ACKNOWLEDGMENTS

This project has received funding from the European Union's Horizon 2020 research and innovation program under grant agreement No. 761030 (CARBAFIN).

DATA AVAILABILITY STATEMENT

Data from the current study are available from doi:10.5281/zenodo.6956069.

ORCID

Bernd Nidetzky http://orcid.org/0000-0002-5030-2643

REFERENCES

Abt, V., Barz, T., Cruz-Bournazou, M. N., Herwig, C., Kroll, P., Möller, J., Pörtner, R., & Schenkendorf, R. (2018). Model-based tools for optimal experiments in bioprocess engineering. *Current Opinion in Chemical Engineering*, *22*, 244–252. https://doi.org/10.1016/j.coche.2018.11.007

Almquist, J., Cvijovic, M., Hatzimanikatis, V., Nielsen, J., & Jirstrand, M. (2014). Kinetic models in industrial biotechnology – improving cell factory performance. *Metabolic Engineering*, *24*, 38–60. https://doi.org/10.1016/j.ymben.2014.03.007

van den Broek, L. A. M., van Boxtel, E. L., Kievit, R. P., Verhoef, R., Beldman, G., & Voragen, A. G. J. (2004). Physico-chemical and transglucosylation properties of recombinant sucrose phosphorylase from *Bifidobacterium adolescentis* DSM20083. *Applied Microbiology and Biotechnology*, *65*(2), 219–227. https://doi.org/10.1007/s00253-003-1534-x

Brucher, B., & Häßler, T. (2019). Enzymatic process for the synthesis of cellobiose. In A. Vogel & O. May (Eds.), *Industrial enzyme applications*. Wiley-VCH Verlag GmbH & Co. KGaA. https://doi.org/10.1002/9783527813780.ch2_4

Clayton, A. D., Schweidtmann, A. M., Clemens, G., Manson, J. A., Taylor, C. J., Niño, C. G., Chamberlain, T. W., Kapur, N., Blacker, A. J., Lapkin, A. A., & Bourne, R. A. (2020). Automated self-optimisation of multi-step reaction and separation processes using machine learning. *Chemical Engineering Journal*, *384*, 123340. https://doi.org/10.1016/j.cej.2019.123340

Domínguez de María, P. (2021). Biocatalysis, sustainability, and industrial applications: Show me the metrics. *Current Opinion in Green and Sustainable Chemistry*, *31*, 100514. https://doi.org/10.1016/j.cogsc.2021.100514

Duong-Trung, N., Born, S., Kim, J. W., Schermeyer, M.-T., Paulick, K., Borisyak, M., Cruz-Bournazou, M. N., Werner, T., Scholz, R., Schmidt-Thieme, L., Neubauer, P., & Martinez, E. (2023). When bioprocess engineering meets machine learning: A survey from the perspective of automated bioprocess development. *Biochemical Engineering Journal*, *190*, 108764. https://doi.org/10.1016/j.bej.2022.108764

Dvorak, P., Kurumbang, N. P., Bendl, J., Brezovsky, J., Prokop, Z., & Damborsky, J. (2014). Maximizing the efficiency of multienzyme process by stoichiometry optimization. *ChemBioChem*, *15*(13), 1891–1895. https://doi.org/10.1002/cbic.201402265

Fitzpatrick, D. E., Battilocchio, C., & Ley, S. V. (2016). A novel Internet-based reaction monitoring, control and autonomous self-optimization platform for chemical synthesis. *Organic Process Research & Development*, *20*(2), 386–394. https://doi.org/10.1021/acs.oprd.5b00313

Galmarini, M. V., Baeza, R., Sanchez, V., Zamora, M. C., & Chirife, J. (2011). Comparison of the viscosity of trehalose and sucrose solutions at various temperatures: Effect of guar gum addition. *LWT - Food Science and Technology*, *44*(1), 186–190. https://doi.org/10.1016/j.lwt.2010.04.021

Gernaey, K. V., Lantz, A. E., Tufvesson, P., Woodley, J. M., & Sin, G. (2010). Application of mechanistic models to fermentation and biocatalysis for next-generation processes. *Trends in Biotechnology*, *28*(7), 346–354. https://doi.org/10.1016/j.tibtech.2010.03.006

Harris, P. R., Grover, M. A., Rousseau, R. W., & Bommarius, A. S. (2022). Selectivity and kinetic modeling of penicillin G acylase variants for the synthesis of cephalexin under a broad range of substrate concentrations. *Biotechnology and Bioengineering*, *119*(11), 3117–3126. https://doi.org/10.1002/bit.28214

Helleckes, L. M., Hemmerich, J., Wiechert, W., von Lieres, E., & Grünberger, A. (2023). Machine learning in bioprocess development: from promise to practice. *Trends in Biotechnology*, *41*(6), 817–835. https://doi.org/10.1016/j.tibtech.2022.10.010

Van Hoorebeke, A., Stout, J., Kyndt, J., De Groeve, M., Dix, I., Desmet, T., Soetaert, W., Van Beeumen, J., & Savvides, S. N. (2010). Crystallization and x-ray diffraction studies of cellobiose phosphorylase from *Cellulomonas uda*. *Acta Crystallographica. Section F, Structural Biology and Crystallization Communications*, *66*(3), 346–351. https://doi.org/10.1107/S1744309110002642

Johannsen, J., Meyer, F., Engelmann, C., Liese, A., Fieg, G., Bubenheim, P., & Waluga, T. (2021). Multi-enzyme cascade reaction in a miniplant two-phase-system: Model validation and mathematical optimization. *AIChE Journal*, *67*(4), e17158. https://doi.org/10.1002/aic.17158

Kadokawa, J. (2016). Precision synthesis of functional polysaccharide materials by phosphorylase-catalyzed enzymatic reactions. *Polymers*, *8*(4), 138. https://doi.org/10.3390/polym8040138

Kara, S., & Rudroff, F. (2021). *Enzyme cascade design and modelling*. Springer International Publishing. https://doi.org/10.1007/978-3-030-65718-5

Kaspar, F., Giessmann, R. T., Hellendahl, K. F., Neubauer, P., Wagner, A., & Gimpel, M. (2020). General principles for yield optimization of nucleoside phosphorylase-catalyzed transglycosylations. *ChemBioChem*, *21*(10), 1428–1432. https://doi.org/10.1002/cbic.201900740

Kitaoka, M. (2015). Diversity of phosphorylases in glycoside hydrolase families. *Applied Microbiology and Biotechnology*, *99*(20), 8377–8390. https://doi.org/10.1007/s00253-015-6927-0

Kitaoka, M., Sasaki, T., & Taniguchi, H. (1992). Conversion of sucrose into cellobiose using sucrose phosphorylase, xylose isomerase and cellobiose phosphorylase. *Journal of the Japanese Society of Starch Science*, *39*(4), 281–283. https://doi.org/10.5458/jag1972.39.281

Kitaoka, M., Sasaki, T., & Taniguchi, H. (1992). Synthetic reaction of *Cellvibrio gilvus* cellobiose phosphorylase. *The Journal of Biochemistry*, *112*(1), 40–44. https://doi.org/10.1093/oxfordjournals.jbchem.a123862

Klimacek, M., Sigg, A., & Nidetzky, B. (2020). On the donor substrate dependence of group-transfer reactions by hydrolytic enzymes: Insight from kinetic analysis of sucrose phosphorylase-catalyzed transglycosylation. *Biotechnology and Bioengineering*, *117*(10), 2933–2943. https://doi.org/10.1002/bit.27471

Kuschmierz, L., Shen, L., Bräsen, C., Snoep, J., & Siebers, B. (2022). Workflows for optimization of enzyme cascades and whole cell catalysis based on enzyme kinetic characterization and pathway modelling. *Current Opinion in Biotechnology*, *74*, 55–60. https://doi.org/10.1016/j.copbio.2021.10.020

Lagerman, C. E., Grover, M. A., Rousseau, R. W., & Bommarius, A. S. (2022). Reactor design and optimization of α-amino ester hydrolase-catalyzed synthesis of cephalexin. *Frontiers in Bioengineering and Biotechnology*, *10*, 826357. https://doi.org/10.3389/fbioe.2022.826357

Lange, J.-P. (2021). Performance metrics for sustainable catalysis in industry. *Nature Catalysis*, *4*(3), 186–192. https://doi.org/10.1038/s41929-021-00585-2

Lencastre Fernandes, R., Bodla, V. K., Carlquist, M., Heins, A.-L., Eliasson Lantz, A., Sin, G., & Gernaey, K. V. (2013). Applying mechanistic models in bioprocess development. In C.-F. Mandenius & N. J. Titchener-Hooker (Eds.), *Measurement, monitoring, modelling and control of bioprocesses* (pp. 137–166). Springer Berlin Heidelberg. https://doi.org/10.1007/10_2012_166

Luley-Goedl, C., & Nidetzky, B. (2010). Carbohydrate synthesis by disaccharide phosphorylases: Reactions, catalytic mechanisms and application in the glycosciences. *Biotechnology Journal*, *5*(12), 1324–1338. https://doi.org/10.1002/biot.201000217

Nidetzky, B., Eis, C., & Albert, M. (2000). Role of non-covalent enzyme-substrate interactions in the reaction catalysed by cellobiose phosphorylase from *Cellulomonas uda*. *Biochemical Journal*, *351*(3), 649–659. https://doi.org/10.1042/bj3510649

Nidetzky, B., Griessler, R., Schwarz, A., & Splechtna, B. (2004). Cellobiose phosphorylase from *Cellulomonas uda*: Gene cloning and expression in *Escherichia coli*, and application of the recombinant enzyme in a 'glycosynthase-type' reaction. *Journal of Molecular Catalysis B: Enzymatic*, *29*(1), 241–248. https://doi.org/10.1016/j.molcatb.2003.11.014

Nishimoto, M. (2020). Large scale production of lacto-N-biose I, a building block of type I human milk oligosaccharides, using sugar phosphorylases. *Bioscience, Biotechnology, and Biochemistry*, *84*(1), 17–24. https://doi.org/10.1080/09168451.2019.1670047

Pandi, A., Diehl, C., Yazdizadeh Kharrazi, A., Scholz, S. A., Bobkova, E., Faure, L., Nattermann, M., Adam, D., Chapin, N., Foroughijabbari, Y., Moritz, C., Paczia, N., Cortina, N. S., Faulon, J.-L., & Erb, T. J. (2022). A versatile active learning workflow for optimization of genetic and metabolic networks. *Nature Communications*, *13*(1), 3876. https://doi.org/10.1038/s41467-022-31245-z

Paschalidis, L., Beer, B., Sutiono, S., Sieber, V., & Burger, J. (2022). Design of enzymatic cascade reactors through multi-objective dynamic optimization. *Biochemical Engineering Journal*, *181*, 108384. https://doi.org/10.1016/j.bej.2022.108384

Pergolizzi, G., Kuhaudomlarp, S., Kalita, E., & Field, R. A. (2017). Glycan phosphorylases in multi-enzyme synthetic processes. *Protein & Peptide Letters*, *24*(8), 696–709. https://doi.org/10.2174/0929866524666170811125109

Petroll, K., Kopp, D., Care, A., Bergquist, P. L., & Sunna, A. (2019). Tools and strategies for constructing cell-free enzyme pathways. *Biotechnology Advances*, *37*(1), 91–108. https://doi.org/10.1016/j.biotechadv.2018.11.007

Rosa, S. S., Nunes, D., Antunes, L., Prazeres, D. M. F., Marques, M. P. C., & Azevedo, A. M. (2022). Maximizing mRNA vaccine production with Bayesian optimization. *Biotechnology and Bioengineering*, *119*(11), 3127–3139. https://doi.org/10.1002/bit.28216

Sampedro, J. G., Rivera-Moran, M. A., & Uribe-Carvajal, S. (2020). Kramers' theory and the dependence of enzyme dynamics on trehalose-mediated viscosity. *Catalysts*, *10*(6), 659. https://doi.org/10.3390/catal10060659

Schwaiger, K. N., Voit, A., Dobiašová, H., Luley, C., Wiltschi, B., & Nidetzky, B. (2020). Plasmid design for tunable two-enzyme co-expression promotes whole-cell production of cellobiose. *Biotechnology Journal*, *15*(11), 2000063. https://doi.org/10.1002/biot.202000063

Schwaiger, K. N., Voit, A., Wiltschi, B., & Nidetzky, B. (2022). Engineering cascade biocatalysis in whole cells for bottom-up synthesis of cello-oligosaccharides: flux control over three enzymatic steps enables soluble production. *Microbial Cell Factories*, *21*(1), 61. https://doi.org/10.1186/s12934-022-01781-w

Segel, I. H. (1993). *Enzyme kinetics: Behavior and analysis of rapid equilibrium and steady-state enzyme systems*. John Wiley & Sons. https://www.wiley.com/en-us/Enzyme+Kinetics:+Behavior+and+Analysis+of+Rapid+Equilibrium+and+Steady+State+Enzyme+Systems-p-9780471303091

Sheldon, R. A., & Woodley, J. M. (2018). Role of biocatalysis in sustainable chemistry. *Chemical Reviews*, *118*(2), 801–838. https://doi.org/10.1021/acs.chemrev.7b00203

Shimada, K., Ichihara, T., Tsumiya, T., Takami, Y., & Fukushima, M. (2009). *Purification method and production method for cellobiose* (US Patent No. US 2009/0281305 A1). U.S. Patent and Trademark Office.

Siedentop, R., Claaßen, C., Rother, D., Lütz, S., & Rosenthal, K. (2021). Getting the most out of enzyme cascades: Strategies to optimize *in vitro* multi-enzymatic reactions. *Catalysts*, *11*(10), 1183. https://doi.org/10.3390/catal11101183

Siedentop, R., & Rosenthal, K. (2022). Industrially relevant enzyme cascades for drug synthesis and their ecological assessment. *International Journal of Molecular Sciences*, *23*(7), 3605. https://doi.org/10.3390/ijms23073605

Siedentop, R., Siska, M., Möller, N., Lanzrath, H., von Lieres, E., Lütz, S., & Rosenthal, K. (2023). Bayesian optimization for an ATP-regenerating *in vitro* enzyme cascade. *Catalysts*, *13*(3), 468. https://doi.org/10.3390/catal13030468

Sigg, A., Klimacek, M., & Nidetzky, B. (2021). Three-level hybrid modeling for systematic optimization of biocatalytic synthesis: α-Glucosyl glycerol production by enzymatic trans-glycosylation from sucrose. *Biotechnology and Bioengineering*, *118*(10), 4028–4040. https://doi.org/10.1002/bit.27878

Sigg, A., Klimacek, M., & Nidetzky, B. (2023). Pushing the boundaries of phosphorylase cascade reaction for cellobiose production I: Kinetic model development. Biotechnology and Bioengineering. https://doi.org/10.1002/bit.28602 Manuscript submitted for publication.

Suzuki, M., Kaneda, K., Nakai, Y., Kitaoka, M., & Taniguchi, H. (2009). Synthesis of cellobiose from starch by the successive actions of two phosphorylases. *New Biotechnology*, *26*(3), 137–142. https://doi.org/10.1016/j.nbt.2009.07.004

Taylor, C. J., Felton, K. C., Wigh, D., Jeraal, M. I., Grainger, R., Chessari, G., Johnson, C. N., & Lapkin, A. A. (2023). Accelerated chemical reaction optimization using multi-task learning. *ACS Central Science*, *9*(5), 957–968. https://doi.org/10.1021/acscentsci.3c00050

Taylor, C. J., Pomberger, A., Felton, K. C., Grainger, R., Barecka, M., Chamberlain, T. W., Bourne, R. A., Johnson, C. N., & Lapkin, A. A. (2023). A brief introduction to chemical reaction optimization. *Chemical Reviews*, *123*(6), 3089–3126. https://doi.org/10.1021/acs.chemrev.2c00798

Telis, V. R. N., Telis-Romero, J., Mazzotti, H. B., & Gabas, A. L. (2007). Viscosity of aqueous carbohydrate solutions at different temperatures and concentrations. *International Journal of Food Properties*, *10*(1), 185–195. https://doi.org/10.1080/10942910600673636

Teshima, M., Willers, V. P., & Sieber, V. (2023). Cell-free enzyme cascades—Application and transition from development to industrial implementation. *Current Opinion in Biotechnology*, *79*, 102868. https://doi.org/10.1016/j.copbio.2022.102868

Ubiparip, Z., De Doncker, M., Beerens, K., Franceus, J., & Desmet, T. (2021). β-glucan phosphorylases in carbohydrate synthesis. *Applied Microbiology and Biotechnology*, *105*(10), 4073–4087. https://doi.org/10.1007/s00253-021-11320-z

Wang, G., Haringa, C., Noorman, H., Chu, J., & Zhuang, Y. (2020). Developing a computational framework to advance bioprocess scale-up. *Trends in Biotechnology*, *38*(8), 846–856. https://doi.org/10.1016/j.tibtech.2020.01.009

Wang, L., Zheng, P., Hu, M., & Tao, Y. (2022). Inorganic phosphate self-sufficient whole-cell biocatalysts containing two co-expressed phosphorylases facilitate cellobiose production. *Journal of Industrial Microbiology and Biotechnology*, *49*(3), 846–856. https://doi.org/10.1093/jimb/kuac008

Woodley, J. M. (2022). Ensuring the sustainability of biocatalysis. *Chemsuschem*, *15*(9), e202102683. https://doi.org/10.1002/cssc.202102683

Wu, S., Snajdrova, R., Moore, J. C., Baldenius, K., & Bornscheuer, U. T. (2021). Biocatalysis: Enzymatic synthesis for industrial applications. *Angewandte Chemie International Edition*, *60*(1), 88–119. https://doi.org/10.1002/anie.202006648

You, C., & Percival Zhang, Y. H. (2017). Biomanufacturing by *in vitro* biosystems containing complex enzyme mixtures. *Process Biochemistry*, *52*, 106–114. https://doi.org/10.1016/j.procbio.2016.09.025

Zhou, Z., Li, X., & Zare, R. N. (2017). Optimizing chemical reactions with deep reinforcement learning. *ACS Central Science*, *3*(12), 1337–1344. https://doi.org/10.1021/acscentsci.7b00492

SUPPORTING INFORMATION

Additional supporting information can be found online in the Supporting Information section at the end of this article.

How to cite this article: Sigg, A., Klimacek, M., & Nidetzky, B. (2024). Pushing the boundaries of phosphorylase cascade reaction for cellobiose production II: Model-based multiobjective optimization. *Biotechnology and Bioengineering*, *121*, 566–579. https://doi.org/10.1002/bit.28601